I&EC research
Industrial & Engineering Chemistry Research
pubs.acs.org/IECR
Article

Solubility, Diffusivity, and Permeability of HFC-32 and HFC-125 in Amorphous Copolymers of Perfluoro(butenyl vinyl ether) and Perfluoro(2,2-dimethyl-1,3-dioxole)

Abby N. Harders, Erin R. Sturd, Luke Wallisch, Hannes Schmidt, Yuniva Mendoza-Apodaca, David R. Corbin, Whitney White, Christopher P. Junk, and Mark B. Shiflett*

Cite This: *Ind. Eng. Chem. Res.* 2023, 62, 4054−4063

Read Online

ACCESS | Metrics & More | Article Recommendations | Supporting Information

ABSTRACT: R-410A, an azeotropic mixture composed of 50 wt % difluoromethane (HFC-32, CH_2F_2) and 50 wt % pentafluoroethane (HFC-125, CHF_2CF_3) used in residential and commercial air-conditioning applications, will be phased down due to the high global warming potential (GWP) of HFC-125. The HFC-32 can be reused in low-GWP blends containing hydrofluoroolefins (HFOs); however, incumbent separation technology, fractional distillation, cannot separate azeotropic mixtures. Membrane technology provides the opportunity to achieve a selective separation of azeotropic HFC refrigerant mixtures with lower energy consumption and capital requirements. This study explores the use of amorphous perfluoropolymers for the separation of R-410A. The permeability, solubility, and diffusivity of HFC-32 and HFC-125 were measured in copolymers of perfluoro(butenyl vinyl ether) (PBVE) and perfluoro(2,2-dimethyl-1,3-dioxole) (PDD). Pure gas permeability of HFC-32 and HFC-125 were measured using a static membrane apparatus and the pressure-rise method. Solubility measurements were obtained using a gravimetric microbalance, and diffusivity was calculated using a Fickian model. The results indicate that a high permeability and selectivity of HFC-32/HFC-125 can be obtained with a 50 wt % PBVE and 50 wt % PDD copolymer and that the separation is diffusion-driven over the entire range of compositions tested.

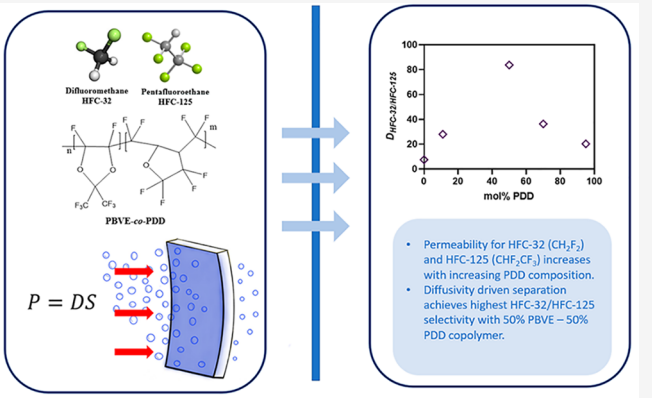

1. INTRODUCTION

Refrigeration and air-conditioning are an integral aspect of modern life. In addition to vapor-compression systems used for refrigeration and air-conditioning, refrigerants are also used as foam blowing agents, aerosols, and fire suppressants.[1] Vapor-compression constitutes 72% of the global end use of fluorocarbon refrigerants, and the technology is deployed in commercial, industrial, transport, and domestic applications.[1] It is estimated that 20% of all energy consumption worldwide can be attributed to the use of refrigeration and air-conditioning.[2] While it is clear that refrigeration and air-conditioning are a necessary technology for modern living, the use of refrigerants has an environmental impact. Hydrofluorocarbons (HFCs) are a class of compounds that are commonly used in refrigeration and air-conditioning systems. HFCs were developed to replace chlorofluorocarbons (CFCs) that were linked to the depletion of the Earth's ozone layer. The Montreal Protocol that was signed in 1987 phased out the use and production of CFCs and hydrochlorofluorocarbons (HCFCs). The Montreal Protocol identified HFCs as a long-term replacement to CFCs and HCFCs.[3] Although the efforts of the Montreal Protocol have been successful in the healing of the ozone layer, some HFCs have high global warming potentials (GWPs) and can trap heat in our atmosphere. In response to the high GWP of some HFCs, the Kyoto Protocol was signed in 1997 and detailed requirements for countries to report their annual HFC emissions to the United Nations Framework Convention on Climate Change.[4] Furthermore, the Kigali amendment was added to the Montreal Protocol in 2016 to provide guidelines on the regulation of HFC production and consumption. It is projected that without the regulations specified by the Kigali amendment, warming of 0.3−0.5 °C would occur by 2100 due to the unregulated use of HFCs.[4] Most recently, the 2020 U.S. American Innovation and Manufacturing (AIM) Act requires a 85% reduction in HFC

Received: December 15, 2022
Revised: January 30, 2023
Accepted: February 3, 2023
Published: February 10, 2023

https://doi.org/10.1021/acs.iecr.2c04518
Ind. Eng. Chem. Res. 2023, 62, 4054−4063

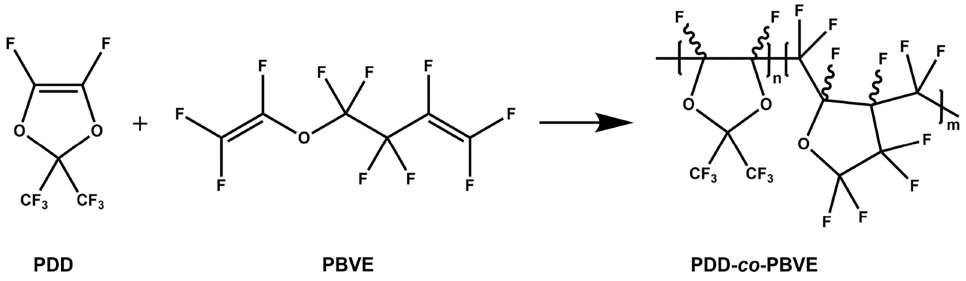

Figure 1. Formation of PBVE-*co*-PDD copolymer from PBVE and PDD.

production by 2035 and implements the international platform of the Kigali Amendment to prevent warming of up to 0.5 °C.[5]

The national and international legislation that calls for the regulation of HFC production and consumption makes the end-of-life handling of HFC refrigerants a timely issue. A substantial amount of HFCs are in circulation around the world. It is estimated that 1000 ktons (1 billion kilograms) of HFCs are in global use.[1] The question of how to handle regulated refrigerants and refrigerant mixtures will have a direct effect on the industries that currently use or produce them. Some widely used HFC mixtures contain components with low GWPs that could be recycled and repurposed into next-generation refrigerants. For example, R-410A is an azeotropic refrigerant mixture composed of 50 wt % difluoromethane (HFC-32, CH_2F_2) and 50 wt % pentafluoroethane (HFC-125, CHF_2CF_3) that provides an opportunity for refrigerant recycle. HFC-32 has a lower GWP (675) than many other HFCs and has the potential to be separated from the R-410A mixture and recycled into next generation refrigerant mixtures containing hydrofluoroolefins (HFOs). In the transition to refrigerants that have zero ozone depletion potential and low global warming potential, HFOs are being considered as the next-generation (i.e., fourth generation) of refrigerants. However, it is important to identify HFC replacements that have similar performance characteristics. HFC/HFO blends can provide low GWP options while maintaining similar performance characteristics to the existing HFC refrigerants. Moreover, retrofitting existing units to HFC/HFO refrigerant mixtures can be a more cost-effective option than conversion to new units, and many of these HFC/HFO blends contain HFC-32. It is estimated that a 40% reduction of global warming impact could be obtained if 60% of the global demand for replacing chlorodifluoromethane (HCFC-22, $CHClF_2$) and R-410A in current applications was met with propane and HFC-32. However, if HFC-32/HFO blends (e.g., R-454B containing 68.9 wt % HFC-32 and 31.1 wt % 2,3,3,3-tetrafluoropropene (HFO-1234yf, $CH_2{=}CFCF_3$) were used instead of pure HFC-32, an 60% reduction (20% additional reduction) of the global warming impact could be realized.[6]

While it is apparent that the ability to separate refrigerant mixtures into their individual components will be important in the coming years, there exists large barriers to these separations due to the presence of azeotropes. Some proposed solutions for the separation of HFCs are the use of ionic liquids as entrainers in extractive distillation columns or selective adsorption using porous materials such as activated carbons, zeolites, and metal organic frameworks.[7−12] An additional separation technology that has been briefly considered in the literature is membrane separation. For example, Pardo et al. has reported on the use of poly(ether-*block*-amide) (PEBA) membranes for the separation of HFC mixtures containing the refrigerants HFC-32, HFC-134a (1,1,1,2-tetrafluoroethane, CH_2FCF_3), and HFO-1234yf.[13] Pardo also reported on the use of composite ionic-liquid/PEBA membranes for the separation of HFC/HFO mixtures.[14] Advantages of membrane technology compared to other technologies include low energy requirements, low operating cost, and compactness.[15] However, drawbacks to membrane separation are the trade-off between permeability and selectivity, lower mass transfer rates compared to other separation technologies, and the risk of plasticization that can lead to reduced selectivity of a membrane over time.[16] In order to overcome these well-known drawbacks, recent advancements in membrane science have shifted toward the development of polymers of intrinsic microporosity, high performance polyimides, thermally rearranged polymers, and amorphous perfluoropolymers.[17] Amorphous perfluoropolymers are unique materials characterized by their resistance to plasticization, chemical stability, and ability to exceed the upper-bounds of selectivity and permeability reported for common gas mixtures. The fluorinated groups within the polymer contain larger covalent radii with fluorine atoms rather than the hydrogen atoms found in hydrocarbon-based polymers. In addition, the C−F bond length is longer in comparison to the C−H bond length.[18] This generally results in lower packing in fluorine containing polymers in comparison to hydrocarbon containing polymer analogues. The larger fractional free volume (FFV) of the amorphous perfluoropolymers allows for higher permeability in comparison to semicrystalline perfluoropolymers such as polytetrafluoroethylene (PTFE).[17,19]

The present study considers the use of perfluoro(butenyl vinyl ether) (PBVE) and perfluoro(2,2-dimethyl-1,3-dioxole) (PDD) copolymers for the separation of HFC-32 and HFC-125 from R-410A. The PDD and PBVE starting materials and the PBVE-*co*-PDD copolymer are shown in Figure 1.

Copolymers of PBVE-PDD provide interesting materials for the separation of gaseous mixtures, due to the ability to adjust the FFV of the copolymer by tuning the amount of PBVE or PDD. Increasing the amount of PDD in the copolymer leads to higher free volume due to the introduction of bulky CF_3 groups, along with greatly restricted rotation around the axis of the polymer backbone. In contast, the PBVE monomer contains less bulky functional groups that allow it to pack more efficiently. A previous study reported on the high selectivity (approximately 13) of HFC-32/HFC-125 with a 5% PBVE−95% PDD copolymer for the separation of R-410A.[20] In order to further assess the use of amorphous perfluoropolymers for the separation of HFC mixtures, the current study reports the pure gas permeability, solubility, and diffusivity of HFC-32 and HFC-125 in five different compositions of PBVE-

https://doi.org/10.1021/acs.iecr.2c04518
Ind. Eng. Chem. Res. 2023, 62, 4054−4063

co-PDD polymers. It should be noted that while this study is focused on the mitigation of climate effects presented by refrigerants, the production of perfluoropolymers has the potential to negatively impact the environment. Although perfluoropolymers are typically considered polymers of low concern in regards to environmental and ecological health, their production can lead to small chain perfluorofluoro alkyl substances being emitted into the environment.[21] Although this is not the focus of this study, this possibility should be considered in any application of this technology or processes involving the production of fluorinated materials.

2. MATERIALS AND METHODS

2.1. Materials. Information about the gases used in this study is provided in Table 1.

Table 1. Gaseous Materials

Gas	CAS no.	Purity
HFC-32, CH_2F_2	75-10-5	>99.9%
HFC-125, CHF_2CF_3	354-33-6	>99.9%
CO_2	124-38-9	>99.995%

HFC-32 and HFC-125 were supplied by the Chemours Company (Newark, DE). CO_2 was purchased from Matheson Tri Gas. The quick-setting epoxy glue was J-B Weld ClearWeld Quick-Setting Epoxy (SKU 50112). PBVE and PBVE-*co*-PDD polymer films were supplied by Chromis Technologies. Physical property data for HFC-32 and HFC-125 were obtained from the National Institute of Standards and Technology (NIST) REFPROP V.10.0 database and are shown in Table 2.

Table 2. Critical Temperature (T_c), Critical Pressure (P_c), Critical Density (ρ_c), Dipole Polarizability (α), Dipole Moment (μ_g), and Molecular Radius (r) of HFC-32 and HFC-125[a]

HFC	T_c (°C)	P_c (MPa)	ρ_c (kg/m^3)	α (Å^3)	μ_g (D)	r (nm)
HFC-32	78.11	5.782	424.00	2.761	1.978	0.16
HFC-125	66.18	3.629	571.30	4.623	1.563	0.23

[a]Critical property data and dipole moments are from Abbott et al. Polarizability values are from Abbott et al. and Gussoni et al. Molecular radius values are from Yokozeki et al.[22−24]

2.2. Methods. *2.2.1. Film Preparation.* The PBVE-*co*-PDD films were prepared by placing a circular shim (5 cm ID, 7 cm OD, 200 μm thick) between two Kapton films on a stainless-steel press measuring 15 cm × 15 cm. The plates were heated to approximately 323 K above the expected glass transition temperature for each polymer sample. The lower plate was then raised until coming into contact with the upper plate. The polymer was heated at this temperature for 5 min, after which the lower plate was raised until approximately 4448 N of force was obtained. The heat was then turned off and the polymer was allowed to cool to ambient temperature over a period of 6 h. After the cooling was complete, the lower plate was lowered to reveal a pressed polymer film approximately 200 μm thick.

2.2.2. Permeability. The separation of gas mixtures through polymeric membranes is a function of solubility and diffusivity as described by the solution-diffusion mechanism. The permeability coefficient, P, characterizes the flux of a permeate through a membrane with a pressure drop, $p_{US} - p_{DS}$, and a thickness, δ.[16] The permeability coefficient for a pure component gas in a static membrane apparatus can be described by the following equation:

$$P = \frac{-V_{DS}\delta}{ARTt} \ln\left(\frac{P_{US} - P_{DS}}{P_{US}}\right) \quad (1)$$

where p_{US} is the upstream pressure, p_{DS} is the downstream pressure, R (m^3 Pa mol^{-1} K^{-1}) is the gas constant, T (K) is the absolute temperature, A is the area of the membrane (m^2), and V_{DS} (m^3) is the downstream volume. The derivation of eq 1 is discussed in detail in the Supporting Information and in a previous reference.[20]

The static membrane apparatus measures the permeability of a gas through a polymeric film adhered to a brass disk mounted over a hole of known area. The operation of the static membrane apparatus has been reported previously;[20] thus only a brief description will be provided here. A polymeric film is placed in the static membrane apparatus such that the downstream and upstream sides of the apparatus are sealed off and the transport of gas can only occur through the polymeric film. The system is pulled under vacuum (<10^{-3} MPa) for a minimum of 12 h in order to remove any volatile impurities. After the system is completely evacuated, the upstream side is pressurized with the permeate gas and maintained at a constant pressure. The gas is then allowed to permeate through the film to the downstream side of the apparatus until a steady-state permeability is reached. Equation 1 is used to calculate the steady-state permeability of the gas through the polymer.

In this study, the pure component permeabilities of HFC-32 and HFC-125 were measured in different compositions of PBVE-*co*-PDD polymers at approximately 0.2 MPa and 308.15 K. Mixed gas selectivity for R-410A in the PBVE-*co*-PDD polymers was also measured with a dynamic mixed-gas permeability apparatus connected to a mass spectrometer (Hiden Isochema Ltd., IGA 003, Warrington, United Kingdom). With the mixed gas apparatus, a membrane was mounted in a similar fashion as with the static membrane apparatus, and the same degassing procedure was followed. R-410A flowed past the membrane at a constant flow rate of 20 SCCM, and the downstream permeate composition was analyzed using a mass spectrometer. The upstream pressure in the module was regulated with a back-pressure regulator to approximately 2 bar. A mixed-gas selectivity was calculated by taking the ratio of the mole fractions of HFC-32/HFC-125 over the ratio of the mole fractions in the permeate stream.

2.2.3. Sorption. A gravimetric microbalance (Hiden Isochema Ltd., IGA 003, Warrington, United Kingdom) with a resolution of 0.0001 mg was utilized to determine HFC-32 and HFC-125 gas absorption into the polymeric films. The gravimetric microbalance measures sample mass variations as a function of pressure, temperature, and gas composition and can be used to determine sorption equilibrium and kinetic parameters.[7] A small rectangular strip (approximately 3.0 cm × 1.0 cm) of polymer film was hung on a tungsten wire using a small copper hook and degassed under vacuum (10^{-7} kPa) at 308.15 K for 24 h to remove volatile impurities. Steady-state mass readings were used to obtain the concentration of the gas in the polymer at each pressure point. The kinetic sorption profile and balance stability were monitored by the HISorp software program, produced by Hiden Isochema.

https://doi.org/10.1021/acs.iecr.2c04518
Ind. Eng. Chem. Res. 2023, 62, 4054−4063

The microbalance was operated in static mode as described in a previous reference.[25] The sample temperature was controlled by a jacketed water bath and measured by an in situ K-type thermocouple (±0.1 K). A platinum resistance thermometer (Hart Scientific SPRT model 5699 and readout Hart Scientific Blackstack model 1560 with a SPRT module 2560) with an accuracy of ±0.005 K was used to calibrate the thermocouple. Note that the gas sorption data was also corrected for volume expansion and buoyancy as described previously.[8,20,25]

2.2.4. Solubility Coefficients. The solubility, S, of each HFC gas is a function of permeate pressure and concentration, as shown in eq 2:

$$S = \frac{C}{p} \tag{2}$$

where p is the permeate pressure and C is the concentration. The solubility at infinite dilution or the solubility coefficient, S^{∞}, is represented as

$$S^{\infty} = \lim_{p\to 0}\left(\frac{C}{p}\right) \approx \left(\frac{dC}{dp}\right)_{p=0} \tag{3}$$

where C is the equilibrium gas concentration at the pressure p. S^{∞} is consistent with the Henry's Law constant, k_H, as shown in eq 4. As the pressure dependence on solubility is considered negligible in most cases, Henry's Law can be utilized to determine the solubility of low-sorbing species in most rubbery polymers at low pressures.

$$C = k_H p \tag{4}$$

In the case of glassy polymers, the solubility of a gas is typically described using the dual mode sorption (DMS) model. The DMS model is a nonpredictive model that has been used to successfully model experimental solubility data for a wide variety of gases in glassy polymers.[26] The model is based on the presence of two populations of sorbed gas within the glassy polymer: a Henry's Law population dissolved within the dense regions of the polymer matrix and a Langmuir population that is characterized by a saturation capacity. The following equation describes this relationship

$$C = k_H p + \frac{C'_H b p}{1 + b p} \tag{5}$$

where the first term describes the Henry's Law population and the second term describes the Langmuir population. The C'_H is the Langmuir capacity constant, and b is the Langmuir affinity constant.

2.2.5. Diffusivity. Using the gravimetric microbalance at 308.15 K and 0.2 MPa, the time-dependent absorption data of HFC-32 and HFC-125 in the PBVE-*co*-PDD films was collected. Fick's Second Law of Diffusion was utilized to model the diffusivity as described by eq 6:

$$\frac{dC}{dt} = D\frac{d^2C}{dx^2} \tag{6}$$

This analysis was described in a previous work, but the theoretical basis will be explained here.[20]

Three assumptions were applied to the system:

(1) a one-dimensional diffusion process describes the dissolution of the gas,
(2) at the interface between the gas and the polymeric film, a thin boundary layer exists where the saturation concentration is instantly established, and
(3) interactions between the polymeric film and the gas are physical.

From these assumptions, three boundary and initial conditions were applied to the system:

$$\text{BC1:}\quad t > 0,\ x = 0,\ \text{and } C = C_s \tag{7}$$

$$\text{BC2:}\quad t > 0,\ x = \frac{L}{2},\ \text{and } \frac{dC}{dx} = 0 \tag{8}$$

$$\text{IC:}\quad t = 0,\ 0 < x < L,\ \text{and } C = C_0 \tag{9}$$

where C is the gas concentration in the polymeric material as a function of time and position, C_s is the saturation concentration, C_0 is the initial concentration, x is the horizontal location, δ is the film thickness, D is the constant diffusion coefficient, and L is the thickness of the sample. A diagram with the corresponding boundary conditions is shown in Figure 2.

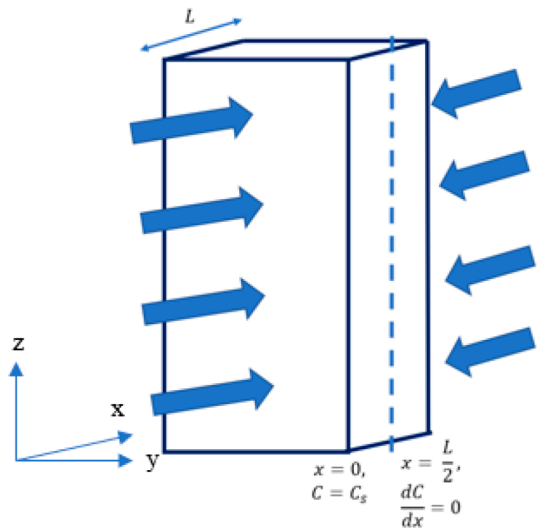

Figure 2. Sample diagram with boundary conditions.

Solving this initial boundary value problem using separation of variables, integrating from 0 to L, and dividing by L yields the average concentration represented by eq 10:

$$\langle C\rangle = C_s + \frac{2}{\pi^2}(C_0 - C_s) \times \sum_{n=0}^{\infty}\left(\frac{(-1)^n - 1}{n^2} e^{-D\pi^2 n^2 t/L^2}(\cos(n\pi) - 1)\right) \tag{10}$$

While there is an infinite summation term in eq 10, the first 20 terms provide adequate numerical accuracy. This diffusion model was fit to experimental concentration data utilizing nonlinear regression and the Levenberg−Marquardt method. The diffusion coefficient (D) and the equilibrium concentration (C_s) were determined using the best fit parameters of this regression.

For systems in which the saturation concentration is reached quickly, nearly all of the absorption from one pressure set point to the next occurs during the ramp in pressure. Thus, the concentration at the beginning of the ramp is significantly

https://doi.org/10.1021/acs.iecr.2c04518
Ind. Eng. Chem. Res. 2023, 62, 4054−4063

smaller than the concentration at the start of the pressure set point, meaning there exists a concentration gradient within the film and the initial condition is not satisfied. Moreover, most of the mass increase happens during the increase in pressure, such that the saturation concentration is reached by the end of the pressure ramp. Equation 9 is a model characterized by initial curvature in the concentration that increases with time and reaches a plateau at the saturation concentration. Under these conditions, the time to reach equilibrium is essentially equivalent to the ramp time, as opposed to the typical diffusion model where the equilibrium time is significantly larger than the time it takes to reach the pressure set point.

In order to model the diffusivity of a gas within a thin film where the saturation concentration is reached quickly, the previous model can be adapted to contain nonconstant boundary conditions to describe diffusion during the ramp. With this adapted model, the concentration at the edges of the film (at $x = 0$ and $x = L$) varies linearly with the increase in pressure and with time. Thus, assumption 2 in the previous model is replaced with the condition that the boundaries of the film are linearly changing concentration until the ramp has reached the set point at $t = t_0$, where t_0 is the ramp time. At the conclusion of the ramp, the boundaries are at the saturation concentration as described by the previous model. Equations 11−13 describe the boundary conditions for this modified model,

$$\text{BC1:} \quad t > 0,\ x = 0,\ \text{and } C = C_0 + \frac{C_s - C_0}{t_0}t \tag{11}$$

$$\text{BC2:} \quad t > 0,\ x = L,\ C = C_0 + \frac{C_s - C_0}{t_0}t \tag{12}$$

$$\text{IC:} \quad t = 0,\ 0 < x < L,\ \text{and } C = C_0 \tag{13}$$

where t is time, t_0 is the total ramp time, C_0 is the concentration at time $t = 0$, C_s is the saturation concentration, and δ is the membrane thickness. Using these nonconstant boundary conditions, eq 6 can be solved to yield an equation for the average concentration in the film during the ramp in pressure.

Through the use of eq 2 and the pure component concentration data, the solubility of a gas at a given composition can be obtained. The diffusion coefficient can be obtained through the process described in eqs 6−13. The permeability can then be calculated using the following relation,

$$P = DS \tag{14}$$

which is a result of the solution-diffusion mechanism that states the permeability is a function of the diffusivity and the solubility. This allows us to calculate the permeability independently from the measured permeability obtained from the pressure-rise method. Both the measured and the calculated permeability will be reported in the following sections.

3. RESULTS

3.1. Single Gas Permeability. The pure-gas permeability of HFC-32 and HFC-125 in the PBVE homopolymer, 89% PBVE−11% PDD, 50% PBVE−50% PDD, 30% PBVE−70% PDD, and 5% PBVE−95% PDD films were measured at 308.15 K and 0.2 MPa using the pressure-rise method. The pure-gas permeability results are reported in Table 3, and the permeability as a function of PDD content is shown in Figure 3. Permeability values are expressed in barrer, where 1 barrer is equivalent to 10^{-10} $\frac{\text{cm}^3_{\text{STP}}\ \text{cm}}{\text{cm}^2\ \text{s cmHg}}$. Permeability results show an increase in permeability for both HFC-32 and HFC-125 when the PDD content in the polymer is increased from 0% to 50%. This is likely due to the increase in FFV of the polymer, which has been stated in the literature to positively impact both solubility and diffusivity of a gas with the absence of specific interactions.[27] For example, this is the case for other fluoropolymers discussed in the literature such as Teflon, Hyflon, and Cytop.[27]

Table 3. Pure-Gas Permeability of HFC-32 and HFC-125 in PBVE-PDD copolymers at 308.15 K and 0.2 MPa

Polymer	*P*: HFC-32 (barrer)	*P*: HFC-125 (barrer)	$\alpha_{\text{HFC-32/HFC-125}}$
PBVE	0.54 ± 0.09	0.12 ± 0.1	5 ± 1
89% PBVE−11% PDD	1.5 ± 0.1	0.29 ± 0.1	5 ± 2
50% PBVE−50% PDD	21 ± 0.1	0.75 ± 0.2	28 ± 7
30% PBVE−70% PDD	53.3 ± 0.1	3.0 ± 0.2	18 ± 1
5% PBVE−95% PDD	361 ± 2	30.0 ± 0.8	12 ± 0.3

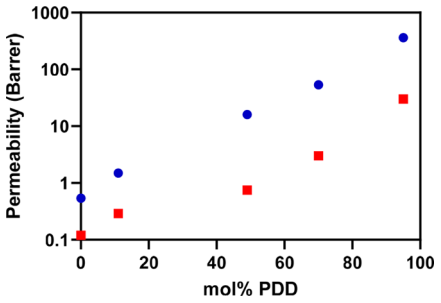

Figure 3. Permeability of HFC-32 (●) and HFC-125 (■) at 308.15 K and 0.2 MPa as a function of PDD composition.

The HFC-32 permeability as a function of PDD exhibits a linear trend when plotted on a logarithmic scale, while the HFC-125 permeability has a slightly nonlinear behavior on the same scale as shown in Figure 3.

The ideal selectivity for this mixture ($P_{\text{HFC-32}}/P_{\text{HFC-125}} = 28$) is maximized at a composition of about 50% PBVE−50% PDD as shown in Figure 4. The ideal selectivity at both 50% PBVE−50% PDD and 30% PBVE−70% PDD compositions are greater than the previously reported selectivity of 12 for the 95 mol % PDD and 5 mol % PBVE composition.[20] However, the permeability at the 50% PBVE−50% PDD is much lower than

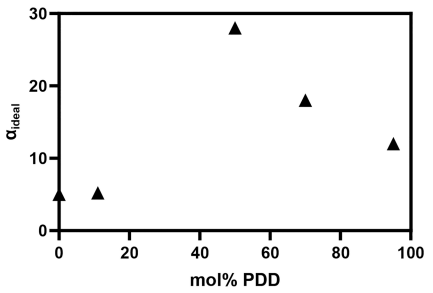

Figure 4. Ideal selectivity ($P_{\text{HFC-32}}/P_{\text{HFC-125}}$) at 308.15 K and 0.2 MPa as a function of PDD composition.

https://doi.org/10.1021/acs.iecr.2c04518
Ind. Eng. Chem. Res. 2023, 62, 4054−4063

the permeability at the 5% PBVE−95% PDD, demonstrating the classic trade-off between permeability and selectivity.

Compositions containing low PDD content are able to chain-pack more efficiently, leading to a smaller amount of FFV and a lower permeability. At low compositions of PDD, chain packing in the copolymer significantly reduces the transport of both HFC-32 and HFC-125. The addition of the PDD monomer increases the FFV and allows for greater HFC transport; however, the rate of increase for HFC-125 permeability is lower than the rate of increase for HFC-32, particularly in the 10−50 mol % PDD copolymer compositions, which results in a maximized selectivity. The selectivity eventually decreases (>50 mol % PDD) as the FFV becomes large enough for high permeability of both gases and an increased rate of HFC-125 permeation. This hypothesis is based on the existence of FFV within the copolymer and the polymer interactions with the HFC gases. Fractional-free volume is commonly estimated in the literature using the Bondi method. The FFV can be calculated using the following relationship:

$$\mathrm{FFV} = 1 - \rho V_o \tag{15}$$

where V_o is the specific occupied volume that is calculated by multiplying 1.3 times the van der Waals volume.[17] The van der Waals volume was calculated for the unit structure based on the method developed in Zhao et al.[28] Due to the nature of this estimation, the FFV exhibits a linear correlation with increasing amounts of PDD and CF_3 groups, as shown in Figure S1 in the Supporting Information.

While this model allows for an idea of how the polymer behaves in regard to dense and voided regions, it is simply based on the presence of functional groups and their occupied volume and fails to capture more intricate interactions between polymer chains. The increasing FFV with PDD content helps to explain the positive correlation between permeability and PDD content within the polymer but fails to explain the nonlinear behavior seen in the HFC-125 permeability that leads to a maximum selectivity at 50 mol % PDD. The more intricate behavior can be further understood with an analysis of the diffusivity and solubility of the gases within the copolymers, which is discussed in the following sections.

Figure 5 compares the permeability of HFC-32 and HFC-125 with the polymer glass transition temperature versus the

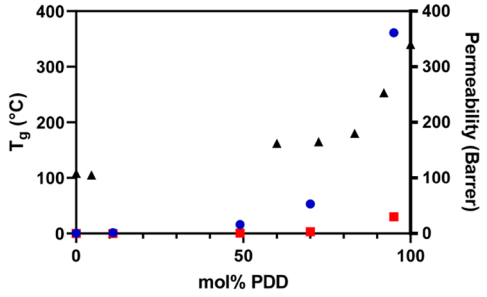

Figure 5. T_g (▲) and permeability of HFC-32 (●) and HFC-125 (■) as a function of PDD composition.

PDD composition. Interestingly, the nonlinear increase in the glass transition temperature that occurs at approximately 70 mol % PDD matches with the large increase in permeability found with HFC-32.

A similar increase in permeability occurs from 70 to 95 mol % PDD with HFC-125; however, the increase is much smaller relative to HFC-32. This behavior suggests that there is a correlation between the glass transition temperature and the permeability. In addition, there is a positive correlation between the FFV of the PBVE-*co*-PDD polymer and the glass transition temperature. White et al. have reported on the linear relationship between FFV and the glass transition temperature for a number of different polymers; however, as shown in Figure 5, there is a nonlinear relationship between the glass transition temperature and the mol % PDD and, thus, a nonlinear relationship between the glass transition temperature and the FFV for these copolymers.

The permeability as a function of the estimated FFV is shown in Figure 6. This trend is nearly identical to the trend

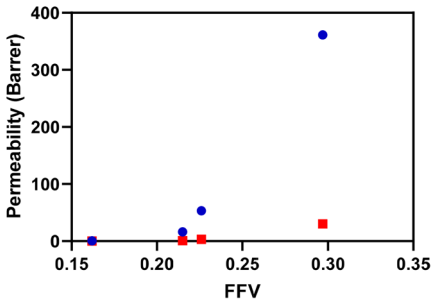

Figure 6. Permeability of HFC-32 (●) and HFC-125 (■) as a function of estimated FFV.

shown in Figure 5 due to the linear relationship between the estimated FFV and the composition of PDD. This suggests that there is a critical free volume (FFV ∼ 0.21) at a composition of about 50% PBVE−50% PDD for optimal size-sieving separation of HFC-32 and HFC-125. For copolymer compositions containing greater than 50 mol % PDD (FFV > 0.21) the effect of size-sieving decreases leading to a lower HFC-32/HFC-125 selectivity.

3.2. Solubility Analysis. The concentration isotherms for HFC-32 and HFC-125 in the PBVE-PDD copolymers at 308.15 K are shown in Figure 7 and Figures S2−S6 in the Supporting Information.

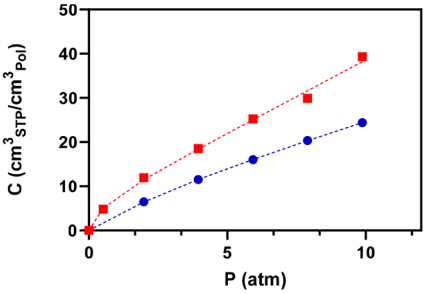

Figure 7. Concentration isotherm of HFC-32 (●) and HFC-125 (■) at 308.15 K in 50% PBVE−50% PDD copolymer.

The isotherms for HFC-32 and HFC-125 in the copolymers (89% PBVE−11% PDD, 50% PBVE−50% PDD, 30% PBVE−70% PDD, and 5% PBVE−95% PDD) were fit to the Dual Mode Sorption model. The isotherms for HFC-32 and HFC-125 in the PBVE homopolymer were linear and able to be fit with the Henry's Law model. For the PBVE homopolymer, the

https://doi.org/10.1021/acs.iecr.2c04518
Ind. Eng. Chem. Res. 2023, 62, 4054−4063

Table 4. Solubility, Diffusivity, and Calculated Permeability of HFC-32 and HFC-125 in PBVE-*co*-PDD Polymers at 308.15 K and 0.2 MPa

Polymer	Gas	S ($cm^3_{(STP)}/(cm^3 \cdot atm)$)	D (10^{-6} cm^2/s)	P_{calc} (barrer)
PBVE	HFC-32	1.29 ± 0.01	3.9 ± 0.2 × 10^{-9}[a]	0.66 ± 0.2
	HFC-125	0.61 ± 0.01	5.2 ± 0.2 × 10^{-10}[a]	0.04 ± 0.01
89% PBVE−11% PDD	HFC-32	1.38 ± 0.01	7.3 ± 0.2 × 10^{-9}[a]	1.33 ± 0.04
	HFC-125	0.83 ± 0.01	2.6 ± 0.2 × 10^{-10}[a]	0.02 ± 0.01
50% PBVE−50% PDD	HFC-32	3.27 ± 0.02	5.7 ± 0.2 × 10^{-8}[a]	25 ± 4
	HFC-125	5.68 ± 0.09	6.8 ± 0.2 × 10^{-10}[a]	0.5 ± 0.08
30% PBVE−70% PDD	HFC-32	3.58 ± 0.04	1.2 ± 0.2 × 10^{-7}[b]	58 ± 10
	HFC-125	6.52 ± 0.04	3.3 ± 0.2 × 10^{-9}[a]	2.83 ± 0.17
5% PBVE−95% PDD	HFC-32	4.61 ± 0.06	6.5 ± 0.2 × 10^{-7}[b]	394 ± 61
	HFC-125	8.80 ± 0.05	3.2 ± 0.2 × 10^{-8}[a]	37 ± 12

[a]Plateau model. [b]Ramp model.

HFC-32 solubility is greater than that of HFC-125, although the opposite is true for the other copolymer compositions tested. The FFV of the PBVE homopolymer is the lowest of all of the polymers tested. As shown in Table 2, the molecular radius of HFC-32 (r = 0.16 nm) is 30% smaller than that of HFC-125 (r = 0.23 nm). It is hypothesized that, due to the tightly packed chains in PBVE and the smaller HFC-32 molecules, HFC-32 is able to transport through the polymer and enter voids that HFC-125 is too large to enter, thus increasing the solubility and transport of HFC-32 relative to HFC-125. For the remaining compositions, the solubility of HFC-125 is greater than that of HFC-32. It has been stated in the literature that gas solubility in a polymer is typically larger for more condensable gases (i.e., gases with a higher T_c).[27] However, the critical temperature of HFC-125 is 339.33 K while the critical temperature of HFC-32 is 351.36 K, indicating that gas condensability cannot explain the solubility trends and that polymer−gas interactions should be considered.[29] Perfluoropolymers have been cited in the literature to have low hydrocarbon solubility in comparison to hydrocarbon-based polymers; therefore, polymer fluorination can be used to tune a HFC separation based on a simple "like-dissolves-like" behavior.[27] If this general rule is applied, then HFC-125 molecules with 2.5 fluorine to carbon atoms (CHF_2CF_3) should exhibit higher solubility than an HFC-32 molecule that contains 2.0 fluorine to carbon atoms (CH_2F_2) in a perfluorinated polymer. Moreover, the hydrogen on the HFC-125 molecule is more labile, contains a partial positive charge, and has the capability of forming hydrogen bonds with the fluorine-containing polymers. The solubilities of HFC-32 and HFC-125 in each polymer at 308.15 K and 0.2 MPa are shown in Table 4. As described with the concentration isotherms, the solubility of HFC-125 is greater than that of HFC-32 at all compositions excluding the PBVE homopolymer. The solubilities for HFC-32 and HFC-125 both increase as a function of PDD content, which is in agreement with the hypothesis that solubility of the HFCs shows a positive correlation with FFV.

The ratio of the HFC-32 and HFC-125 solubilities decreases as a function of the PDD content and eventually reaches a plateau at compositions greater than 50 mol % PDD, as shown in Figure 8. These results indicate that the highest solubility selectivity ($S_{HFC\text{-}32/HFC\text{-}125} \sim 2$) occurs at low amounts of PDD and that a separation based on differences in solubility is not feasible for this copolymer. The solubility of HFC-32 and HFC-125 as a function of PDD content is shown in Figure S7 in the Supporting Information.

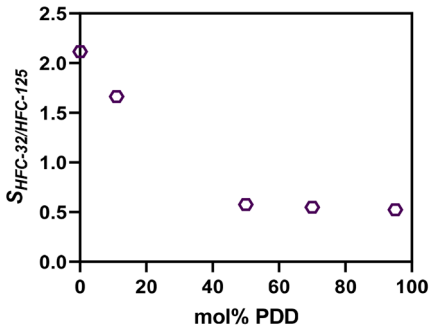

Figure 8. Solubility ratio of HFC-32/HFC-125 at 308.15 K and 0.2 MPa as a function of PDD composition.

The solubility coefficients at infinite dilution for HFC-32 and HFC-125 in each polymer are shown in Table S7 in the Supporting Information. In general, the solubility of HFC-32 and HFC-125 in the polymer increases with increasing PDD content, although the solubilities at infinite dilution for 50% PBVE−50% PDD and 30% PBVE−70% PDD compositions are quite similar. The lower solubility at infinite dilution for HFC-32 in the 89% PBVE−11% PDD polymer may be due to limitations in the ability to accurately measure the extremely small mass changes associated with HFC-32, coupled with the uncertainty in the linear fit used to approximate the solubility at infinite dilution for these two copolymers. Except in the case of the PBVE homopolymer, the solubility at infinite dilution for HFC-125 was higher than that of HFC-32 in the copolymers. This is in overall agreement with what is shown with the concentration isotherms in Figures S2−S6 in the Supporting Information.

3.3. Diffusion Analysis. To validate the pressure-ramp model that contains nonconstant boundary conditions, the diffusion coefficient for HFC-32 was obtained by fitting the general, constant boundary condition model and the pressure-ramp model to experimental sorption data. The 30% PBVE−70% PDD system was chosen to illustrate the agreement between both models (i.e., constant boundary condition model or "plateau model" and nonconstant boundary condition model or "pressure-ramp model"). The diffusivity of HFC-32 was modeled at 308.15 K and 0.2 MPa to capture the plateau model. The pressure-ramp model was illustrated by ramping the pressure from 0 to 0.2 MPa at 308.15 K and fitting the nonconstant boundary condition model to the experimental concentration data. Using the ramp model as shown in Table 4, the diffusion coefficient was calculated to be 1.2 ± 0.2 ×

https://doi.org/10.1021/acs.iecr.2c04518
Ind. Eng. Chem. Res. 2023, 62, 4054−4063

10^{-7} cm^2/s, and with the plateau model, the diffusion coefficient was calculated to be $1.7 \pm 0.2 \times 10^{-7}$ cm^2/s. This result shows that both the ramp and the plateau models are in good agreement, indicating the validity in the pressure-ramp model in the absence of data suitable for modeling with eq 10.

For further verification of our modeling process, the concentration of CO_2 was measured as a function of time in the 50% PBVE−50% PDD copolymer and the diffusion coefficient was modeled by fitting the experimental sorption data to the modified Fickian model. The result was then compared to the diffusion coefficient reported in Okazy et al.[30] The measured diffusion coefficient is $1.6 \pm 0.3 \times 10^{-6}$ cm^2/s, and the literature diffusion coefficient is $1.1 \pm 0.3 \times 10^{-6}$ cm^2/s. The diffusion coefficient for CO_2 in this work is in good agreement with the diffusion coefficient reported in the literature, indicating validity of our model with what is reported in the literature.

Table 4 contains the diffusion coefficients for HFC-32 and HFC-125 in all PBVE and PBVE-*co*-PDD polymers. As a general rule, increasing amounts of PDD leads to an increase in gas diffusivity due to increasing FFV of the polymer. The diffusion coefficients span 3 orders of magnitude for HFC-32 (10^{-9}−10^{-7} cm^2/s) and HFC-125 (10^{-10}−10^{-8} cm^2/s) over the range of PDD compositions tested (i.e., 0% PDD to 95% PDD). It should be noted that the diffusion coefficient for HFC-125 in the 89% PBVE−11% PDD composition is slightly lower than the diffusion coefficient modeled for the PBVE homopolymer as shown in Figure S8 in the Supporting Information. This result was not expected based on the trend of diffusivity increasing with increasing FFV and may be due to the small mass uptake and quantitatively fitting a model at low pressures.

The ratio of the diffusion coefficients of HFC-32 and HFC-125 as a function of PDD content is shown in Figure 9. The

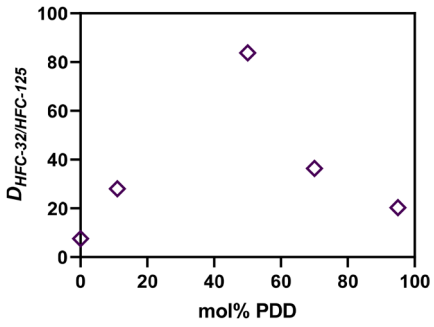

Figure 9. Diffusivity ratio of HFC-32/HFC-125 at 308.15 K and 0.2 MPa as a function of PDD composition.

ideal selectivity trend shown in Figure 4 follows the diffusion ratio trends. The diffusion ratios are greater than 1 for the entire composition range and reach a maximum of 83 at the 50 mol % PDD composition. These results indicate a diffusivity-driven separation for the PBVE-*co*-PDD polymers. The diffusion coefficients for HFC-125 and HFC-32 as a function of PDD composition are shown in Figure S8 in the Supporting Information. Given the logarithmic axis, the HFC-32 diffusivity follows a linear relationship with PDD composition. The HFC-125 diffusivity remains relatively constant until reaching a composition of about 50 mol % PDD and then increases linearly with increasing PDD composition. Within experimental uncertainty the diffusivity of HFC-125 in the PBVE homopolymer and 89% PBVE−11% PDD copolymer are relatively the same.

3.4. Permeability and Selectivity Analysis. The measured and calculated permeabilities for HFC-32 and HFC-125 are reported in Table 5. There is overall a good

Table 5. Measured and Calculated Permeability at 308.15 K and 0.2 MPa

Polymer	Penetrant	P_{calc} (barrer)	P_{meas} (barrer)
PBVE	HFC-32	0.66 ± 0.2	0.54 ± 0.09
	HFC-125	0.04 ± 0.01	0.12 ± 0.02
89% PBVE−11% PDD	HFC-32	1.33 ± 0.04	1.5 ± 0.1
	HFC-125	0.02 ± 0.01	0.29 ± 0.1
50% PBVE−50% PDD	HFC-32	25 ± 4	21 ± 0.3
	HFC-125	3.66 ± 0.06	1.42 ± 0.04
30% PBVE−70% PDD	HFC-32	94 ± 5	53.3 ± 0.1
	HFC-125	1.54 ± 0.86	4.48 ± 0.06
5% PBVE−95% PDD	HFC-32	394 ± 61	361 ± 2
	HFC-125	37 ± 12	30.0 ± 0.8

agreement between the measured permeability and the calculated permeability for all compositions tested. Differences between the measured and calculated permeabilities may be a result of the measured permeability being more prone to defects in the membrane, any presence of adhesive on the membrane surface, or defects in the seal. As seen within the composition range of 50−70 mol % PDD, the calculated permeability is larger than what is measured with the static membrane apparatus.

A comparison of the "calculated" selectivity using the measured solubility and diffusivity versus the "measured" selectivity using the pure HFC permeances is shown in Figure 10. Both the calculated and the measured selectivities follow a

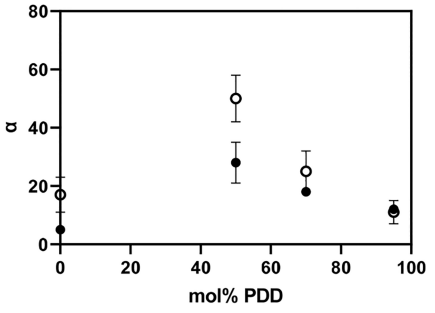

Figure 10. Calculated (○) and measured (●) selectivity at 308.15 K and 0.2 MPa as a function of PDD composition.

similar trend with the maximum selectivity occurring at the 50% PBVE−50% PDD composition. The calculated selectivity was in most cases higher than the measured selectivity based on the ratio of the pure HFC permeance measurements, which was expected due to the ideal nature of the calculated measurements and may be an indication of the maximum selectivity ($\alpha = 50$) possible with this copolymer for separating HFC-32/HFC-125.

3.5. Mixed Gas Measurements. The mixed gas HFC-32/HFC-125 selectivity, or separation factor, was also measured for three of the copolymers. The flow rate was maintained at 20 SCCM, the upstream pressure was maintained at 2 bar, and the membrane area was identical to what was used in the

https://doi.org/10.1021/acs.iecr.2c04518
Ind. Eng. Chem. Res. 2023, 62, 4054−4063

single-gas permeation experiments. The mixed gas selectivity in 95% PBVE−5% PDD was 5 ± 0.3, compared to the ideal selectivity of 5 ± 1 for the PVE homopolymer. The mixed gas selectivity in 50% PBVE−50% PDD was 26 ± 2, compared to the ideal selectivity of 28 ± 7. The mixed gas selectivity in 5% PBVE−95% PDD was 13.9 ± 0.8, compared to the ideal selectivity of 12 ± 0.3. It should be noted that the driving forces for permeation in terms of partial pressure between the single gas permeability experiments (HFC-32 and HFC-125 total pressures at 0.2 MPa) and the mixed gas experiments (total pressure at 0.2 MPa, HFC-32 partial pressure at 0.6 MPa and HFC-125 partial pressure at 1.4 MPa) are different. The agreement illustrates that transport of the individual HFC gases through the fluorinated copolymers is not significantly influenced by the presence of the other gas; therefore, gas−polymer interactions are more significant than HFC−HFC interactions.

Pardo et al. reported the permeability of HFC-32 and HFC-125 in neat Pebax membrane of approximately 7 and Pebax-ionic liquid (1-ethyl-3-methylimidazolium thiocyanate) mixed-matrix membranes with a selectivity of 14.[31] The selectivity for HFC-32/HFC-125 in the 50% PBVE−50% PDD copolymer is 28 and surpasses what has been previously reported in the literature for this mixture. In terms of permeability, the Pebax-ionic liquid membrane exhibits an HFC-32 permeability of approximately 250 barrer. The 5% PBVE−95% PDD film has a selectivity nearly identical to the Pebax-ionic liquid membrane with a higher permeability of approximately 360 Barrer.

4. CONCLUSION

The efficient separation of azeotropic refrigerant mixtures such as R-410A and others has become an important issue for reclaiming and recycling HFC refrigerants. Membrane technology provides a possible solution for refrigerant reclaimers to separate azeotropic refrigerant mixtures that cannot be separated using incumbent technology based on fractional distillation. The current study investigates the solubility, diffusivity, permeability, and selectivity of HFC-32 and HFC-125 in five amorphous fluoropolymer membranes composed of PBVE and copolymers of PBVE and PDD. Increasing the PDD composition led to increases in both HFC-32 and HFC-125 permeability, which is a function of increasing fractional free volume. Increasing the PDD composition also increases the HFC-125 solubility relative to HFC-32, and a maximum in the diffusivity ratio of HFC-32 to HFC-125 occurs at about 50% PBVE and 50% PDD. The diffusion-driven separation results in a maximum selectivity of about 28 for HFC-32 over HFC-125 using a 50% PBVE−50% PDD copolymer. This composition provides the highest selectivity; however, if higher HFC-32 permeability is required, the PDD content should be increased. Mixed gas selectivity results are in good agreement with the ideal selectivity, indicating no presence of plasticization or reduced selectivity due to HFC−HFC interactions. In summary, a 50% PBVE−50% PDD copolymer currently exhibits the highest membrane selectivity for R-410A reported in the literature, making it a potential commercial material for this separation.

■ ASSOCIATED CONTENT

Supporting Information

The Supporting Information is available free of charge at https://pubs.acs.org/doi/10.1021/acs.iecr.2c04518.

Figure S1, fractional free volume as a function of PDD content; Table S1, isothermal absorption data for HFC-32 and HFC-125 in PBVE at 308.15 K; Figure S2, concentration isotherm of HFC-32 and HFC-125 at 308.15 K in PBVE homopolymer; Table S2, isothermal absorption data for HFC-32 and HFC-125 in 89% PBVE−11% PDD at 308.15 K; Table S3, isothermal absorption data for HFC-32 and HFC-125 in 50% PBVE−50% PDD at 308.15 K; Figure S4, concentration isotherm of HFC-32 and HFC-125 at 308.15 K in 50% PBVE−50% PDD copolymer; Table S4, isothermal absorption data for HFC-32 and HFC-125 in 30% PBVE−70% PDD at 308.15 K; Figure S5, concentration isotherm of HFC-32 and HFC-125 at 308.15 K in 30% PBVE−70% PDD copolymer; Table S5, isothermal absorption data for HFC-32 and HFC-125 in 5% PBVE−95% PDD at 308.15 K; Figure S6, concentration isotherm of HFC-32 and HFC-125 at 308.15 K in 5% PBVE−95% PDD copolymer; Table S6, dual mode sorption parameters of HFC-32 and HFC-125 at 308.15 K and 0.2 MPa; Table S7, infinite dilution solubility coefficients of HFC-32 and HFC-125 at 308.15 K; Figure S7, solubility of HFC-32 and HFC-125 at 308.15 K and 0.2 MPa as a function of PDD content; Figure S8, diffusivity of HFC-32 and HFC-125 at 308.15 K and 0.2 MPa as a function of PDD content; and Figure S9, thin film diagram for permeability derivation (PDF)

■ AUTHOR INFORMATION

Corresponding Author

Mark B. Shiflett − *Institute for Sustainable Engineering, University of Kansas, Lawrence, Kansas 66045, United States;* orcid.org/0000-0002-8934-6192; Email: mark.b.shiflett@ku.edu

Authors

Abby N. Harders − *Institute for Sustainable Engineering, University of Kansas, Lawrence, Kansas 66045, United States;* orcid.org/0000-0003-0311-3855

Erin R. Sturd − *Institute for Sustainable Engineering, University of Kansas, Lawrence, Kansas 66045, United States;* orcid.org/0000-0003-0606-1018

Luke Wallisch − *Institute for Sustainable Engineering, University of Kansas, Lawrence, Kansas 66045, United States*

Hannes Schmidt − *Institute for Sustainable Engineering, University of Kansas, Lawrence, Kansas 66045, United States*

Yuniva Mendoza-Apodaca − *Meredith College, Raleigh, North Carolina 27607, United States*

David R. Corbin − *Institute for Sustainable Engineering, University of Kansas, Lawrence, Kansas 66045, United States*

Whitney White − *Chromis Technologies, Warren, New Jersey 07059, United States*

Christopher P. Junk − *Chromis Technologies, Warren, New Jersey 07059, United States*

Complete contact information is available at: https://pubs.acs.org/10.1021/acs.iecr.2c04518

Notes

The authors declare no competing financial interest.

https://doi.org/10.1021/acs.iecr.2c04518
Ind. Eng. Chem. Res. 2023, 62, 4054−4063

REFERENCES

(1) Booten, C. W.; Nicholson, S. R.; Mann, M. K.; Abdelaziz, O. *Refrigerants: Market Trends and Supply Chain Assessment*; U.S. Department of Energy: 2020; DOI: 10.2172/1599577.

(2) McLinden, M. O.; Huber, M. L. (R)Evolution of Refrigerants. *J. Chem. Eng. Data* **2020**, *65* (9), 4176−4193.

(3) Calm, J. M. The next Generation of Refrigerants - Historical Review, Considerations, and Outlook. *Int. J. Refrig.* **2008**, *31* (7), 1123−1133.

(4) Flerlage, H.; Velders, G. J. M.; de Boer, J. A Review of Bottom-up and Top-down Emission Estimates of Hydrofluorocarbons (HFCs) in Different Parts of the World. *Chemosphere* **2021**, *283*, 131208.

(5) EPA. *Protecting Our Climate by Reducing Use of Hydrofluorocarbons Proposed Rule-Phasedown of Hydrofluorocarbons: Establishing the Allowance Allocation and Trading Program under the American Innovation and Manufacturing Act*; 2021.

(6) Zeiger, B.; Gschrey, B.; Schwarz, W. *Alternatives to HCFCs/HFCs in Developing Countries with a Focus on High Ambient Temperatures*; Öko-Recherche: 2014.

(7) Morais, A. R. C.; Harders, A. N.; Baca, K. R.; Olsen, G. M.; Befort, B. J.; Dowling, A. W.; Maginn, E. J.; Shiflett, M. B. Phase Equilibria, Diffusivities, and Equation of State Modeling of HFC-32 and HFC-125 in Imidazolium-Based Ionic Liquids for the Separation of R-410A. *Ind. Eng. Chem. Res.* **2020**, *59*, 18222−18235.

(8) Shiflett, M. B.; Yokozeki, A. Solubility and Diffusivity of Hydrofluorocarbons in Room-Temperature Ionic Liquids. *AIChE J.* **2006**, *52* (3), 1205−1219.

(9) Shiflett, M. B.; Scurto, A. M. Ionic Liquids: Current State and Future Directions. In *Ionic Liquids: Current State and Future Directions*; ACS Symposium Series; American Chemical Society: 2017; Vol. *1250*, pp 1−13, DOI: 10.1021/bk-2017-1250.ch001.

(10) Yancey, A. D.; Terian, S. J.; Shaw, B. J.; Bish, T. M.; Corbin, D. R.; Shiflett, M. B. A Review of Fluorocarbon Sorption on Porous Materials. *Microporous Mesoporous Mater.* **2022**, *331*, 111654.

(11) Asensio-Delgado, S.; Pardo, F.; Zarca, G.; Urtiaga, A. Absorption Separation of Fluorinated Refrigerant Gases with Ionic Liquids: Equilibrium, Mass Transport, and Process Design. *Sep. Purif. Technol.* **2021**, *276*, 119363.

(12) Baca, K. R.; Olsen, G. M.; Matamoros Valenciano, L.; Bennett, M. G.; Haggard, D. M.; Befort, B. J.; Garciadiego, A.; Dowling, A. W.; Maginn, E. J.; Shiflett, M. B. Phase Equilibria and Diffusivities of HFC-32 and HFC-125 in Ionic Liquids for the Separation of R-410A. *ACS Sustain. Chem. Eng.* **2022**, *10* (2), 816−830.

(13) Pardo, F.; Zarca, G.; Urtiaga, A. Separation of Refrigerant Gas Mixtures Containing R32, R134a, and R1234yf through Poly(Ether-Block-Amide) Membranes. *ACS Sustain Chem. Eng.* **2020**, *8* (6), 2548−2556.

(14) Pardo, F.; Gutiérrez-Hernández, S. v.; Zarca, G.; Urtiaga, A. Toward the Recycling of Low-GWP Hydrofluorocarbon/Hydrofluoroolefin Refrigerant Mixtures Using Composite Ionic Liquid-Polymer Membranes. *ACS Sustain. Chem. Eng.* **2021**, *9* (20), 7012−7021.

(15) Abedini, R.; Nezhadmoghadam, A. Application of Membrane In Gas Separation Processes: Its Suitability and Mechanisms. *Pet. Coal* **2010**, *52* (2), 69−80.

(16) Yampolskii, Y. Polymeric Gas Separation Membranes. *Macromolecules* **2012**, *45* (8), 3298−3311.

(17) El-Okazy, M. A.; Liu, L.; Junk, C. P.; Kathmann, E.; White, W.; Kentish, S. E. Gas Separation Performance of Copolymers of Perfluoro(Butenyl Vinyl Ether) and Perfluoro(2,2-Dimethyl-1,3-Dioxole). *J. Membr. Sci.* **2021**, *634*, 119401.

(18) Okamoto, Y.; Chiang, H.-C.; Merkel, T. Perfluoropolymers for Membrane Application. In *Fascinating fluoropolymers and their applications*; Ameduri, B., Fomin, S., Eds.; Elsevier: 2020; pp 143−148.

(19) El-Okazy, M. A.; Liu, L.; Abdellah, M. H.; Goudeli, E.; Kentish, S. E. Gas Sorption and Diffusion in Perfluoro(Butenyl Vinyl Ether) Based Perfluoropolymeric Membranes. *J. Membr. Sci.* **2022**, *644*, 120095.

(20) Harders, A. N.; Sturd, E. R.; Vallier, J. E.; Corbin, D. R.; White, W. R.; Junk, C. P.; Shiflett, M. B. Selective Separation of HFC-32 from R-410A Using Poly(Dimethylsiloxane) and a Copolymer of Perfluoro(Butenyl Vinyl Ether) and Perfluoro(2,2-Dimethyl-1,3-Dioxole). *J. Membr. Sci.* **2022**, *652*, 120467.

(21) Lohmann, R.; Cousins, I. T.; Dewitt, J. C.; Glüge, J.; Goldenman, G.; Herzke, D.; Lindstrom, A. B.; Miller, M. F.; Ng, C. A.; Patton, S.; Scheringer, M.; Trier, X.; Wang, Z. Are Fluoropolymers Really of Low Concern for Human and Environmental Health and Separate from Other PFAS? *Environ. Sci. Technol.* **2020**, *54* (20), 12820−12828.

(22) Abbott, A. P.; Eardley, C. A.; Tooth, R. Relative Permittivity Measurements of 1,1,1,2-Tetrafluoroethane (HFC 134a), Pentafluoroethane (HFC 125), and Difluoromethane (HFC 32). *J. Chem. Eng. Data* **1999**, *44*, 112.

(23) Gussoni, M.; Rui, M.; Zerbi, G. Electronic and Relaxation Contribution to Linear Molecular Polarizability. An Analysis of the Experimental Values. *J. Mol. Struct.* **1998**, *447* (3), 163−215.

(24) Yokozeki, A.; Sato, H.; Watanabe, K. Ideal-Gas Heat Capacities and Virial Coefficients of HFC Refrigerants. *Int. J. Thermophys.* **1998**, *19* (1), 89−127.

(25) Minnick, D. L.; Turnaoglu, T.; Rocha, M. A.; Shiflett, M. B. Review Article: Gas and Vapor Sorption Measurements Using Electronic Beam Balances Cite As: *J. Vac. Sci. Technol. A* **2018**, *36*, 050801.

(26) Ricci, E.; de Angelis, M. G. Modelling Mixed-Gas Sorption in Glassy Polymers for CO2 Removal: A Sensitivity Analysis of the Dual Mode Sorption Model. *Membranes 2019, Vol. 9, Page 8* **2019**, *9* (1), 8.

(27) Merkel, T. C.; Pinnau, I.; Prabhakar, R.; Freeman, B. D. Gas and Vapor Transport Properties of Perfluoropolymers. *Materials Science of Membranes for Gas and Vapor Separation* **2006**, 251−270.

(28) Zhao, Y. H.; Abraham, M. H.; Zissimos, A. M. Fast Calculation of van Der Waals Volume as a Sum of Atomic and Bond Contributions and Its Application to Drug Compounds. *J. Org. Chem.* **2003**, *68* (19), 7368−7373.

(29) Schmidt, J. W.; Moldover, M. R. Alternative Refrigerants CH2F2 and C2HF5: Critical Temperature, Refractive Index, Surface Tension, and Estimates of Liquid, Vapor, and Critical Densities. *J. Chem. Eng. Data* **1994**, *39* (1), 39−44.

(30) El-Okazy, M. A.; Liu, L.; Junk, C. P.; Kathmann, E.; White, W.; Kentish, S. E. Gas Separation Performance of Copolymers of Perfluoro(Butenyl Vinyl Ether) and Perfluoro(2,2-Dimethyl-1,3-Dioxole). *J. Membr. Sci.* **2021**, *634*, 119401.

(31) Pardo, F.; Zarca, G.; Urtiaga, A. Effect of Feed Pressure and Long-Term Separation Performance of Pebax-Ionic Liquid Membranes for the Recovery of Difluoromethane (R32) from Refrigerant Mixture R410A. *J. Membr. Sci.* **2021**, *618*, 118744.

https://doi.org/10.1021/acs.iecr.2c04518
Ind. Eng. Chem. Res. 2023, 62, 4054−4063